J Mater Sci: Mater Med (2010) 21:3109–3118
DOI 10.1007/s10856-010-4163-9

Image processing and fractal box counting: user-assisted method for multi-scale porous scaffold characterization

Vincenzo Guarino · Angela Guaccio · Paolo A. Netti · Luigi Ambrosio

Received: 18 March 2010 / Accepted: 21 September 2010 / Published online: 5 October 2010

Abstract Image analysis has gained new effort in the scientific community due to the chance of investigating morphological properties of three dimensional structures starting from their bi-dimensional gray-scale representation. Such ability makes it particularly interesting for tissue engineering (TE) purposes. Indeed, the capability of obtaining and interpreting images of tissue scaffolds, extracting morphological and structural information, is essential to the characterization and design of engineered porous systems. In this work, the traditional image analysis approach has been coupled with a probabilistic based percolation method to outline a general procedure for analysing tissue scaffold SEM micrographs. To this aim a case study constituted by PCL multi-scaled porous scaffolds was adopted. Moreover, the resulting data were compared with the outputs of conventionally used techniques, such as mercury intrusion porosimetry. Results indicate that image processing methods well fit the porosity features of PCL scaffolds, overcoming the limits of the more invasive porosimetry techniques. Also the cut off resolution of such IP methods was discussed. Moreover, the fractal dimension of percolating clusters, within the pore populations, was addressed as a good indication of the interconnection degree of PCL bi-modal scaffolds. Such findings represent (i) the bases for a novel approach complementary to the conventional experimental procedure used for the morphological analysis of TE scaffolds, in particular offering a valid method for the analysis of soft materials (i.e., gels); also (ii) providing a new perspective for further studies integrating to the structural and morphological data, fluid-dynamics and transport properties modelling.

V. Guarino (✉) · L. Ambrosio
Institute for Composite and Biomedical Materials (IMCB-CNR), P.le Tecchio 80, Naples, Italy
e-mail: vguarino@unina.it

A. Guaccio (✉) · P. A. Netti
Interdisciplinary Research Centre on Biomaterials CRIB and Italian Institute of Technology IIT, P.le Tecchio 80, Naples, Italy
e-mail: angela.guaccio@unina.it

1 Introduction

Image Processing (IP) has been developed in the past decades as a challenging approach to a number of applications in a wide variety of fields [1]. The main reason is that, today, visual information instruments such as high computational power microcomputer, digital cameras, image digitizer and image processing tools are often low cost and available consumer goods. Typically, IP deals with two dimensional discrete mapping used as representation of three-dimensional real objects. Each point holds a number of information in terms of intensity, amplitude, and grey level colour, carrying, in turn, morphological and structural knowledge. Therefore, the IP process takes image or image sequence as input and produces as output a set of parameters and function related to the content of images. The central step to get from the input to the output is constituted by a series of operators or processing techniques. These concern the modulation of brightness and contrast, binary operations involving 8-bit images, complex processes in the Fourier space and methods for quantitatively measuring image contents. For example, bulk properties of three dimensional samples, were determined by extracting correlation function from the images and applying them to statistical analyses of the sample [2]. Thus far, it was possible to calculate porosity, chord length distribution, pore size distribution and coarseness, as well

as pore connectivity degree, and to correlate these to physical properties of fluid flow dynamics [2–4]. Recently, IP methods have been adopted to characterize the structure and the bulk properties of scaffolds for Tissue Engineering (TE) applications [5].

The more common approaches are based on the use of X-ray based microtomography, which allows the reproduction of the complex three dimensional trabecular architecture of TE scaffolds [6–15], scanning electron microscopy (SEM) [16–19] and confocal laser scanning microscopy [18]. In particular, scanning electron microscopy (SEM) analysis offers a qualitative evaluation of hierarchically complex porous scaffolds providing a direct measurements of strut/wall thickness and a visual estimation of pore size, interconnectivity, cross-section area and anisotropy [20]. Once collected the micrographs, image analysis efficiency is highly dependent on the image contrast, image resolution and analysis methods used to segment the image [15, 21]. In particular, image segmentation results a crucial point in the outcome of structural analysis. Indeed, the main problem is the partitioning of an image into meaningful pieces or, alternatively, the confinement of regions of interest (i.e. pores and/or trabeculae). The ideal case consists of two distinct intensity distributions, the one for the pores and the other for the polymer continuous phase. However, the more complex is the structure the less defined are the two distributions [22], and the more challenging is the application of robust and efficient algorithm for image segmentation. Thus far, up to date, it has not yet been developed any image processing technique to provide accurate image segmentation not affected by image variability. To help with this, several researchers have proposed mechanisms for validating the effectiveness of various segmentation algorithms [23, 24]. One strategy consists in quantifying the general behaviour of the algorithm relative to an ideal reference model, which is, usually, hand contouring one slice at time by expert observers (manual segmentation) [25]. Thus a study may use hand-contouring results to asses the performance of a segmentation technique. This paper takes such approach, and provides general shape metrics to compare results of an edge-based algorithm for segmentation, implemented on porous Poly ε-caprolactone scaffolds by a self-implemented Matlab code (Matlab v.7.0), with the computer-aided manual segmentation (NIH ImageJ v.3.7). Once segmented, scaffold images may be broken up in their partition of voids and strut, and scaffold characteristic features may be extracted. Among the others, the interconnection degree (ID) of scaffolds represents a key parameter in the definition of scaffold architecture functionality for tissue engineering. Indeed, the spatial and topological arrangement of pores within the structures is fundamental to provide fluid flow, i.e. nutrient supply and waste removal, and tissue in-growth [26]. In particular, an open interconnected porous network enhances the exchange of nutrients and waste materials with the environment [26–28], while a lack of pore interconnection may hinder cell proliferation and even promote cell death [29]. From the image analysis point of view, the existence of interconnections implies the presence of percolative pathways made of black-void pixels within the white polymer matrix. Here, it has been proposed the fractal dimension of such percolating patterns as an indication for scaffold ID.

The aim of the work is, therefore, to provide a schematic representation of an IP algorithm for the complete characterization of polymeric structures as scaffold for TE applications. To this aim, in the following sections it has been described the methods adopted for scaffold preparation, and data collection and analysis; further, the results of these studies have been critically discussed in comparison with conventionally used experimental techniques, and the implication for future tests have been summarized.

2 Materials and methods

2.1 Scaffold fabrication

PCL scaffolds have been prepared by thermally induced phase separation and salt leaching technique. Briefly, Poly ε-caprolactone pellets (Sigma-Aldrich M_W 65 kDa) were dissolved in absolute Dioxane (Sigma-Aldrich, purity 99.5%) by stirring for about 3 h at room temperature up to form a homogeneous solution. Three different polymer/solvent weight ratio were selected, 05/95, 15/85 and 30/70 (wt/wt), respectively. NaCl particles, sieved into a size ranges of 300–500 μm, were mixed to the polymer solution by using volume ratio of PCL/NaCl, 09/91 (v/v). The mixture was placed into Teflon mould and cylindrical disks (14 mm in diameter, 3 mm in thickness) were carried out by fast quenching down to (−18 ± 1)°C. Solvent removal was allowed in pure ethanol (C_2H_5OH) bath at atmospheric pressure and −18°C for 48 h. Ethanol solution was changed daily for a more efficacious dioxane extraction. The complete elimination of the volatile components (ethanol and dioxane residuals), by evaporation, was let under chemical hood for 3 h. Finally, all specimens were placed in bi-distilled water for 7 days to leach out sodium chloride crystals and any other contaminants. The complete evaporation of the adsorbed water was assured by keeping samples under hood for about 3 h.

2.2 Scaffold imaging

Scanning Electron Microscopy (SEM, Stereoscan 440, Leica Oxford, UK) was used to capture image of scaffolds

along their longitudinal and cross sections. A scalpel blade was used to cut the scaffolds along the vertical axis of cylinders. Each sample was mounted on an aluminium stub, by using an adhesive carbon tab, and sputter coated with gold, under vacuum, before imaging. Images were digitized on a matrix of 1,024 * 1,024 pixels with 256 grey levels in the tagged image file format (TIFF).

2.3 Image processing

Image analysis procedure has been reported step by step in the schematic representation of Fig. 1, in agreement with the ASTM F2603-06 (Standard Guide 2007). Primarily, *image selection* was performed based on the criteria of image similarity in terms of magnification, brightness and contrast, information reported on the micrograph raw data. Three images of the same polymer scaffold were chosen for each magnification. Once captured an image can be manipulated as it follows. First scaffold images were converted to monochrome that spans a grey scale ranging from near black to near white (*pre-elaboration)*. The conversion of images into binary form (8-bit conversion) reduces the calculation complexity. In detail, the "*image binarization*" will output a monochromatic image with 256 levels composed of pure black pixels (level 0) and pure white pixels (level 1) which cover the 256 grey level of the original image. With this transformation the void and the solid component of the samples, respectively level 0 and level 1 of the binary images, result represented by the values at the opposite ends of the greyscale. Intermediate shades of grey represent the transition in brightness that occurs as the solid component terminates into pores. The next step consists of the establishment of a criterion for segmentation of images, by distinguishing between solid (*wall*) and voids (*pore*) phases, respectively. In this phase, filtering procedures by image smoothing and sharpening, the adjustment of contrast/brightness and the adequate definition of the grey threshold level was needful to evidence the pores respect to the polymer matrix and eliminate artefacts which could negatively affect next calculations. At this time the procedure split into two direction.

On one side, the individuation of voids was performed manually (hand contouring), even if the procedure presented some difficulties due to the complexity of structures that hindered the proper definition of pore boundaries. Afterwards, the images were analysed by the use of ImageJ software and porosity degree, pore size and spatial distribution were derived by using the "*particle analysis*" tools contained into ImageJ software pack: this provides the tracing of the entire inter-phase boundaries related to the pore walls, and then, the counting of all pore object, calculating quantitatively their size and their surface area. The porosity degree was evaluated from the total surface area of counted pores whereas the pore sizes were derived.

In the Matlab routine the threshold level was set, by using the criteria of edge detection (ED), on a single greyscale value, after stepping it to investigate upon the threshold value effect on porosity calculation [22, 26]. This approach was used for separating touching objects without a subjective threshold, i.e. depending upon a visual inspection of the investigator [8]. For the evaluation of micro and macropores, the analyses were performed by selecting an adequate size range of the object to count (region-based approach), according to the characteristic pore sizes reported in other works [30, 31]. Specifically, the analysis was based on the assumption that a surface of 1,000 μm^2 defines the boundary line between micropores and macropores. In both cases, it might be uncertainty in the measured values due to ambiguities in the edge object recognition, homogeneity in the size and shape of pores, and their orientation with respect of the images. The values calculated on three different samples have been reported as mean ± standard deviations (SD).

2.4 Mercury intrusion porosimetry

Pore features were also determined by mercury intrusion porosimetry (Thermo Electron Pascal 140–240) according

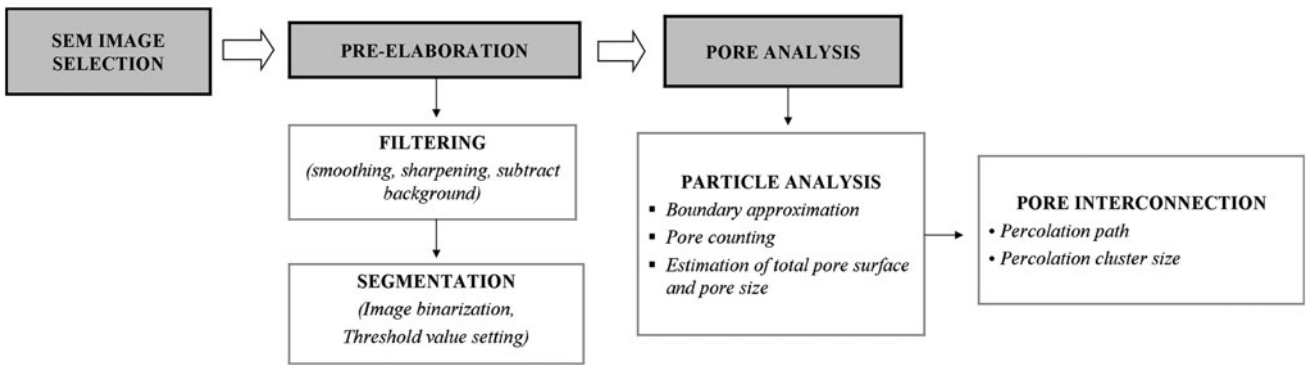

Fig. 1 Schematic flow chart of the image processing algorithm

to the Washburn equation [19] which allows to correlate: the applied pressure on the intrusion fluid, the pore radius, the surface tension of the mercury and the contact angle between mercury and polymer. In particular, a mercury surface tension of 480 mN/m and a contact angle of 141.3° were imposed, while p_{max} equal to 400 Pa and 200 kPa, respectively, was applied in conjunction to pore size analysis. This method yields the total porosity, expressed as a percentage value, simultaneously to the average pore diameter. As a consequence, the elaboration of data in the light of the Washburn equation allows to build the pore size distribution.

2.5 Estimation of pore interconnection degree

Interconnection degree of scaffolds was evaluated by calculating the fractal dimension, D, of percolating clusters through the use of freeware ImageJ plugin based on the box counting method. In the simplest terms, the routine counts the number of boxes of a given size needed to cover a one pixel wide, binary (black on white) border. The procedure is repeated for boxes that are 2–64 pixels wide. The output consists of two columns representing the size and the boxes number (count) needful to cover the borders. A plot is generated with the log of size on the *x* axis and the log of count on the *y* axis, while the data are fitted with a straight line. Line slope (S) represents the fractal dimension (D) [32].

3 Result and discussions

SEM images of PCL scaffolds with different polymer/solvent ratio have been analysed by IP techniques, to derive morphological and structural information (Fig. 2a, c). Visual inspections of images allow the identification of the porous and polymeric phases, as well as, of a bimodal porous structure where macropores, with irregular shape, coexist with micropores, located along the trabeculae. A remarkable reduction of micropores occurs with increasing the polymer concentration, because of a progressive reduction of capability of the polymer system to de-mixing during the phase separation [33]. Image segmentation is essential to discriminate between the void and the polymeric phase. The complexity of structures is well represented by the intensity histograms of the original SEM micrographs relative to 5/95 and 30/70 (wt/wt) polymer concentrations, respectively (Fig. 2b, d). As expected, histograms of real images are characterized by two distribution, of voids and strut, merging in an intermediate gray shade, between the two peaks of black (voids) and white (strut). The more effective is the segmentation algorithm adopted, the more distinct would be the two intensity distributions [22]. Noteworthy, SEM images show highly asymmetric intensity distribution with an evident peak at zero, corresponding to the black pixels, and the second peak corresponding to the trabecular structure, more evident as the volume of solvent increases. Such findings may

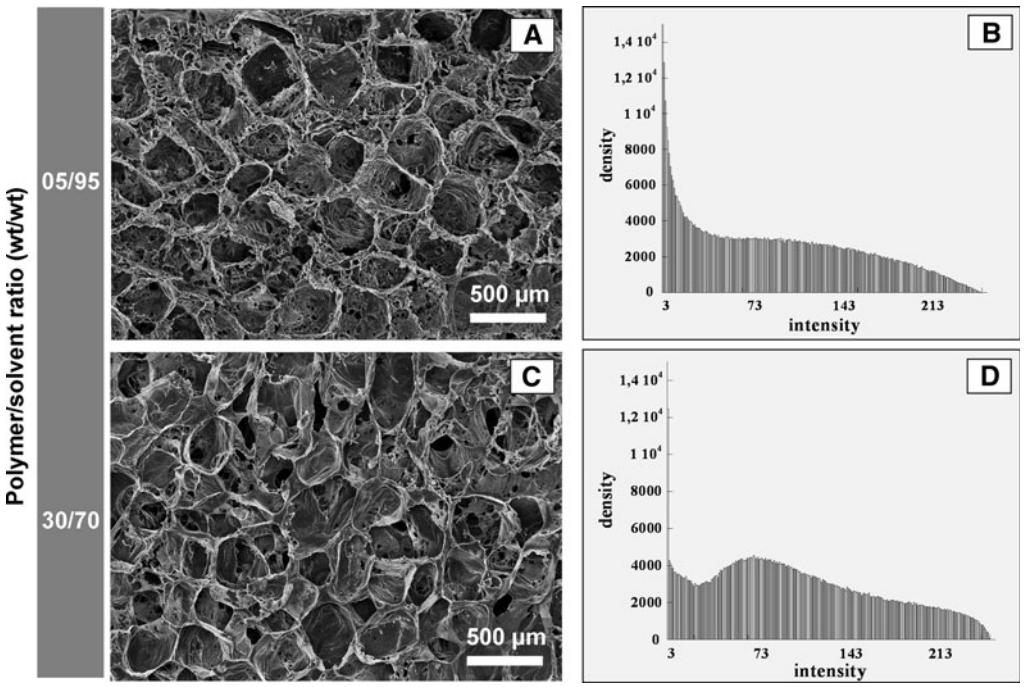

Fig. 2 Segmentation based on threshold selection: selected images of PCL scaffolds with PCL/dioxane weight ratio at 05/95 (wt/wt) (**a**) and 30/70 (wt/wt) (**c**) and relative histograms of intensity (**b**, **d**)

be addressed to the presence of visible micropores affecting the strut wall, in the 05/95 (wt/wt) scaffolds, which results in more frequent boundary regions, associated to gray scale pixels, respect to the white peak of continuous polymer matrix. Conversely, in the 70/30 (wt/wt) scaffolds, white regions, related to scaffold struts in the images, are well identified and the separation between the two phases is more evident.

Before segmentation, all datasets have been processed to reduce noise and smooth homogeneous regions. The smoothing pre-processing step reduces the time necessary to perform the segmentation by decreasing sensitivity to small scale features and texture, also removing the noise and enhancing edges. Binary images derived by this pre-elaboration step have been reported in Fig. 3a–d. Finally, to assist in the identification of pore boundaries, an assigned limiting dimension for macro- and micropores has been defined for each sample, addressing to macropores as pores of about 30 μm average diameter, while to micropores as pores of few microns in size.

Figure 4 is a comparison of the results of a typical ED-based segmentation (Matlab algorithm) with a typical manual segmentation, for each porous population. The surface of the respective experimental and manual masks are rendered in figure a–d and e–f. Images show that the elaboration failed in areas where there was not enough colour contrast with surrounding structure for the algorithm to detect an edge (Fig. 4a, e). Such weak edges, however, were also difficult to visualize for manual segmentation. This yields thinner trabecular segments and less defined pore shapes within the macropore population (Fig. 4a, b and e, f). In Table 1, the average pore dimensions and the porosity degree, carried out by the using of the proposed segmentation methods, have been reported. Results show that there is not any significant difference about macropore characteristics, strictly related only to the porogen used for both scaffold composition. Furthermore, the two methods demonstrated a good agreement with respect to the calculated values (SD = ±0.1–1.3). In the micro-pores population, as expected, the porosity percentage is varying with polymer concentration, with a reduction of about 65% from the 05/95 (wt/wt) to the 30/70 (wt/wt) PCL scaffolds.

Besides, a multi-population of pores is strongly desired in order to assure nutrient transport and waste removal within the scaffold, but even cell growth and migration, processes favoured by a higher surface/volume ratio [34]. Concerning the effect of polymer/solvent ratio on the average pore size, data indicate that the macro-pores population is constituted by greater pores for the 05/95 (wt/wt) respect to the 30/70 (wt/wt) scaffolds—an increment of approximately 17% of the mean value—with the good agreement of the manual segmentation. Such results may be explained with the effect of segregation between salt crystals allowed by the less viscous solution [35]. Finally,

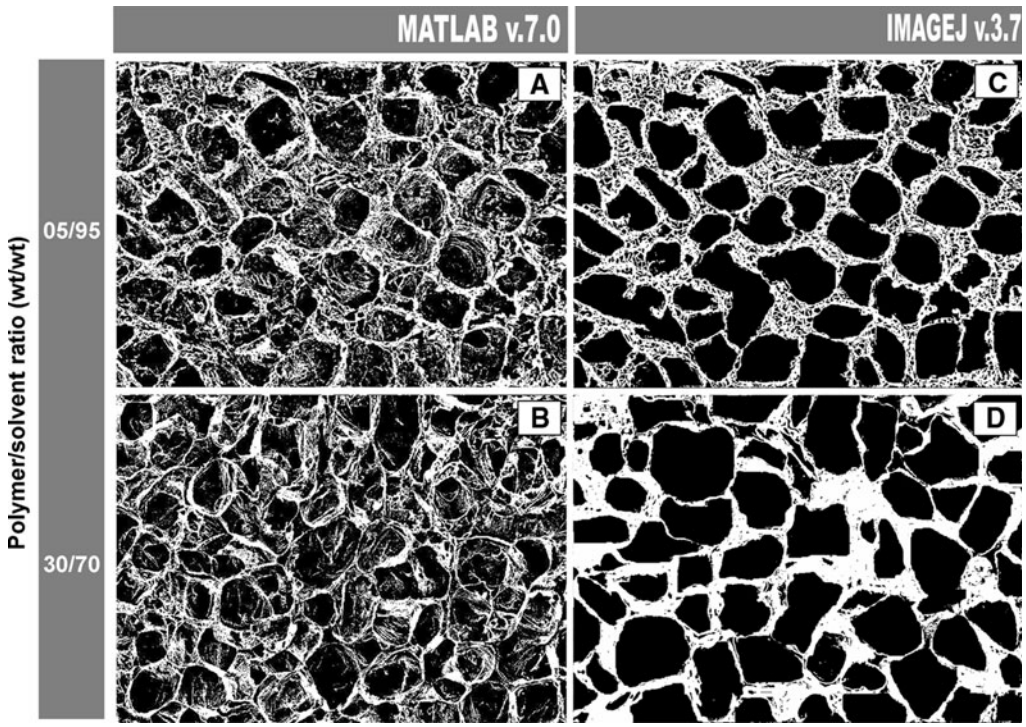

Fig. 3 Image segmentation based on threshold selection of PCL scaffolds with PCL/dioxane weight ratio at 05/95 (wt/wt) (**a**, **c**) and 30/70 (wt/wt) (**b**, **d**): 8-bit images by Matlab code (**a**, **b**) and Image J (**c**, **d**) manipulation

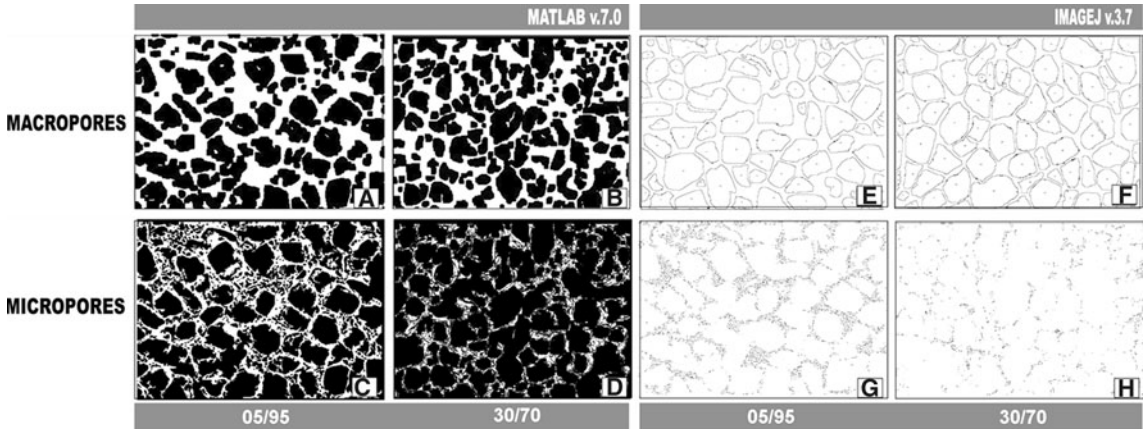

Fig. 4 Pore analysis on PCL scaffolds with PCL/dioxane weight ratio at 05/95 (wt/wt) and 30/70 (wt/wt): boundary definition and pore counting of macropores and micropores by Matlab (**a–d**) and Image J (**e–h**) procedure

Table 1 Summary of porosity and pore size of micropores (<1,000 μm^2) and macropores (>1,000 μm^2) obtained by user-assisted image processing

PCL/dioxane weight ratio	Porosity (%)		Average pore size (μm)	
	Macro	Micro	Macro	Micro
05/95	71.2 ± 0.5	6.46 ± 0.8	190 ± 8	12 ± 2
30/70	71.5 ± 1.3	1.91 ± 0.1	157 ± 17	11 ± 4

the high standard deviation for micropores probably depends on the image resolution, for that micro-pores have sizes comparable with the pixels of images and this may determine a source of error. It is worth to note that in many cases the manual segmentation extends beyond object boundaries indicated by sharp changes in colour or contrast. This trend explains much of the discrepancy between the manual and Matlab-ED segmentation, but it also brings into question the usefulness of these manual segmentation as ground truth. Thus far, two main points need to be discussed, if IP processing might represent a method for overcoming the limits of traditionally well known techniques, and if these resulting data may be extended to the 3D pore volume properties.

Traditionally, scaffold properties have been measured essentially by indirect methods, based on the evaluation of volume capacity of pores (mercury intrusion porosimetry, MI) or weight loss from the bulk to the porous constructs (i.e., gravimetric methods) [36]. However the most diffused method of fluid intrusion porosimetry for studying porous materials [37], fails for soft scaffolds such as flexible foams (with porosities higher than 90%) due to the application of high pressures (up to 400 MPa). This may provoke the pore structure collapse which compromises the entire scaffold architecture and therefore the measurements [36]. Moreover, this technique underestimates porosity by neglecting

Table 2 Comparison of porosity and pore size data calculated by IP and MI techniques

Measure Method	PCL/dioxane weight ratio	Porosity (micro and macro) (%)	Average pore size (micro/macro) (μm)
IP	15/85	76.65 (71.86 + 4.79)	(10.6/180.9)
MI	15/85	77.58	121.63

closed pores, since the fluid does not intrude into them, preventing a quantitative estimation of further basic structural parameters, such as pore interconnectivity, strut/wall thickness and pore anisotropy. Therefore, the adoption of optical techniques able to compute digitally images integrated with analytical procedures for the definition of morphological cues is a promising alternative approach. In Table 2 it has been reported the comparison between IP and MI results, for calculation of porosity features of PCL scaffolds. While IP methods allow the definition of a macro- and a micro-pore separated distributions (Fig. 5a, b), the MI porosimetry measurements individuate a wider porosity distribution characterized by the presence of several peaks (Fig. 5c) associated to the intruded macroporosities, with an average value intermediate between the media of micro and of macropores, derived by IP measurements, and a lower average pore size (Table 2). This is ascribable to the partial collapse of pore architecture during the mercury intrusion under vacuum as just suggested in other works [16]. Conversely, no relevant mismatch has been evidenced in terms of total porosity degree. Noteworthy, the analysis has been conducted only in the case of scaffolds with intermediate microporous values, corresponding to 15/85 (wt/wt) PCL/dioxane ratio, as compromise solution between scaffold softness and pore interconnectivity.

On the other hand, while MI represents a method of investigation of a 3D structure, image analysis techniques

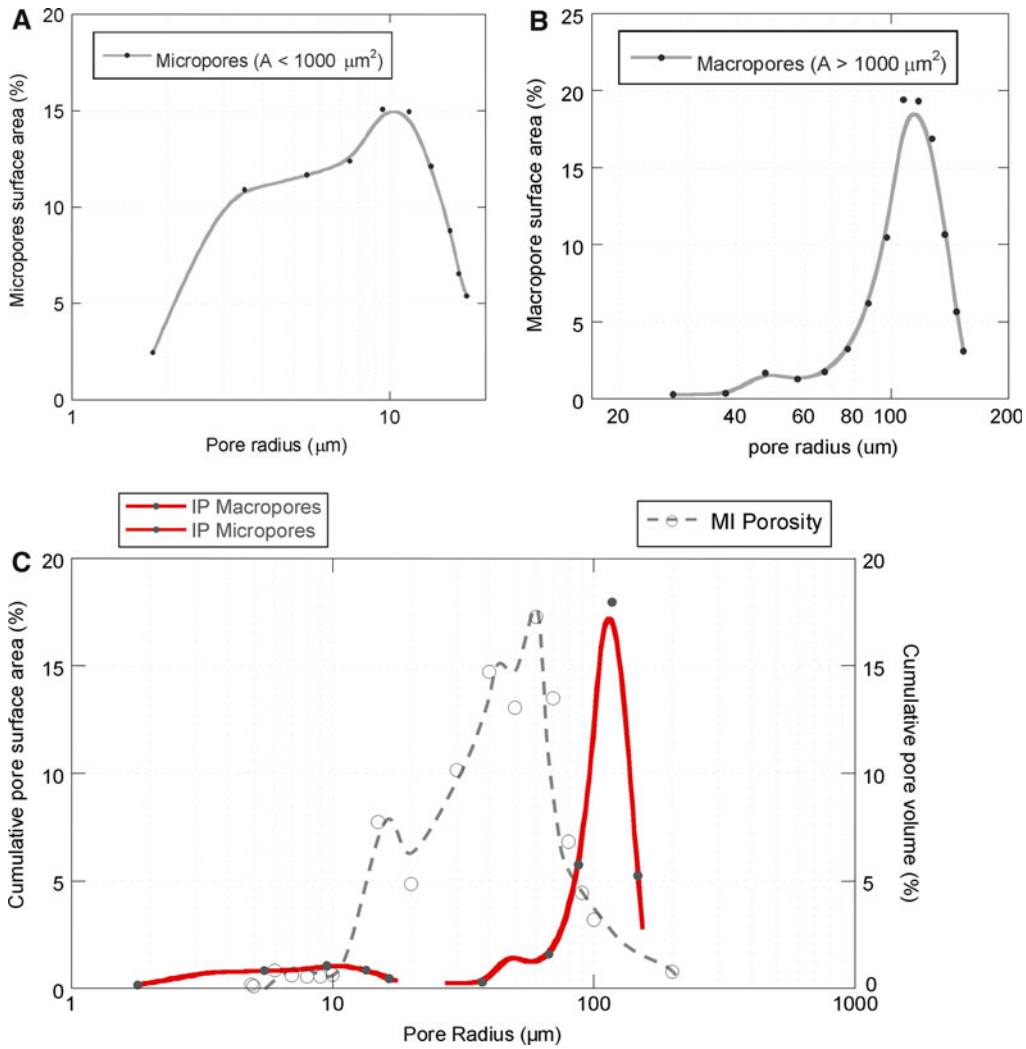

Fig. 5 IP analysis of PCL scaffolds with 15/85 PCL/dioxane ratio (wt/wt): micropore (**a**) and macropore (**b**) surface distribution curves. **c** Overlapping of pore surface and pore volume cumulative distribution by IP and MI techniques, respectively

are based on two dimensional cross section analysis. Such limit may explain the reason why IP processing technique may be considered not convincing as instruments for quantitative evaluation of scaffold features, among the scientific community. To overcome such limits, up to date, the three dimensional structures, have been investigated only by a computer aided reconstruction mainly based on μ-CT experiments [38]. Nonetheless, predicting 3D pore features from 2D data has been addressed from many researcher for sand stones [39]. Two basic underlying assumption in these studies are (i) the structure of the sand stone is homogeneous and isotropic, and (ii) the 2D image covers an area large enough to avoid that the microscopic variability dominate the prediction. In other words, for regions larger enough than the "*representative elementary region*" or region of interest (ROI), average properties are independent of the area—properties of self-similarity—and reflects the values for the bulk volume [40]. For sand stone, it has been observed that the length of four grain diameters is the length scale required to obtain a stable asymptotic value for porosity properties and is the same minimum length scale for porosity determined for glass beads [41]. The image size required to reach a stable, asymptotic value, however may not be the same for porosity, permeability and tortuosity factor, i.e. the region whose properties may be extended to the bulk volume depends on the property measured [42]. Based upon these findings, in this study, a ROI with size of 300 × 300 μm was selected as representative of the morphological properties of PCL scaffolds. A proper choice of the ROI of 2D images allows the extension to the 3D structure of the features calculated herein. In particular it is interesting to evaluate the interconnection degree of scaffolds by starting from their bi-dimensional representation.

In order to overcome the relevant limitation of traditional approaches on the quantification of the interconnectivity

degree, recently, it has been demonstrated that percolation model may be successfully used to extract additive information about pore interconnectivity from 2D images of 3D scaffolds [43]. Some applications of percolation model to image processing have been attempted previously [44, 45]. However, they were limited to determine the parameters of an existing image processing method, or to detect global fluid flow in an image [46]. The percolation is a physical model based on the natural phenomenon of the permeation of liquid into porous networks [46]. The basic concept is that, once identified a starting point for the penetration of fluid within a porous matrix, it is possible to estimate the most probable pathway for fluid flow. The process starts by assigning a probability value P to each point close to the first, based on a specific characteristic (pore dimension, morphology of pore boundaries), and identifying as second the point with the highest probability among the neighbourhood. The assigned probability P is a measure of the "*ease of percolation*" where points which exhibit the largest value of P describe the percolation path. Noteworthy, the percolation pathway is always constituted by interconnected pores. To implement the percolation theory in image processing, the probability P is assigned as a function of the brightness range in scaffold images, so that only the nearest pixels with brightness ranging in a defined interval have the higher probability to be percolated and to form clusters. Thus far, it is possible to associate the fractal dimension of percolating cluster to the interconnection degree of a structure [47]. Indeed, the closer is the fractal dimension to the geometric dimension of the object under

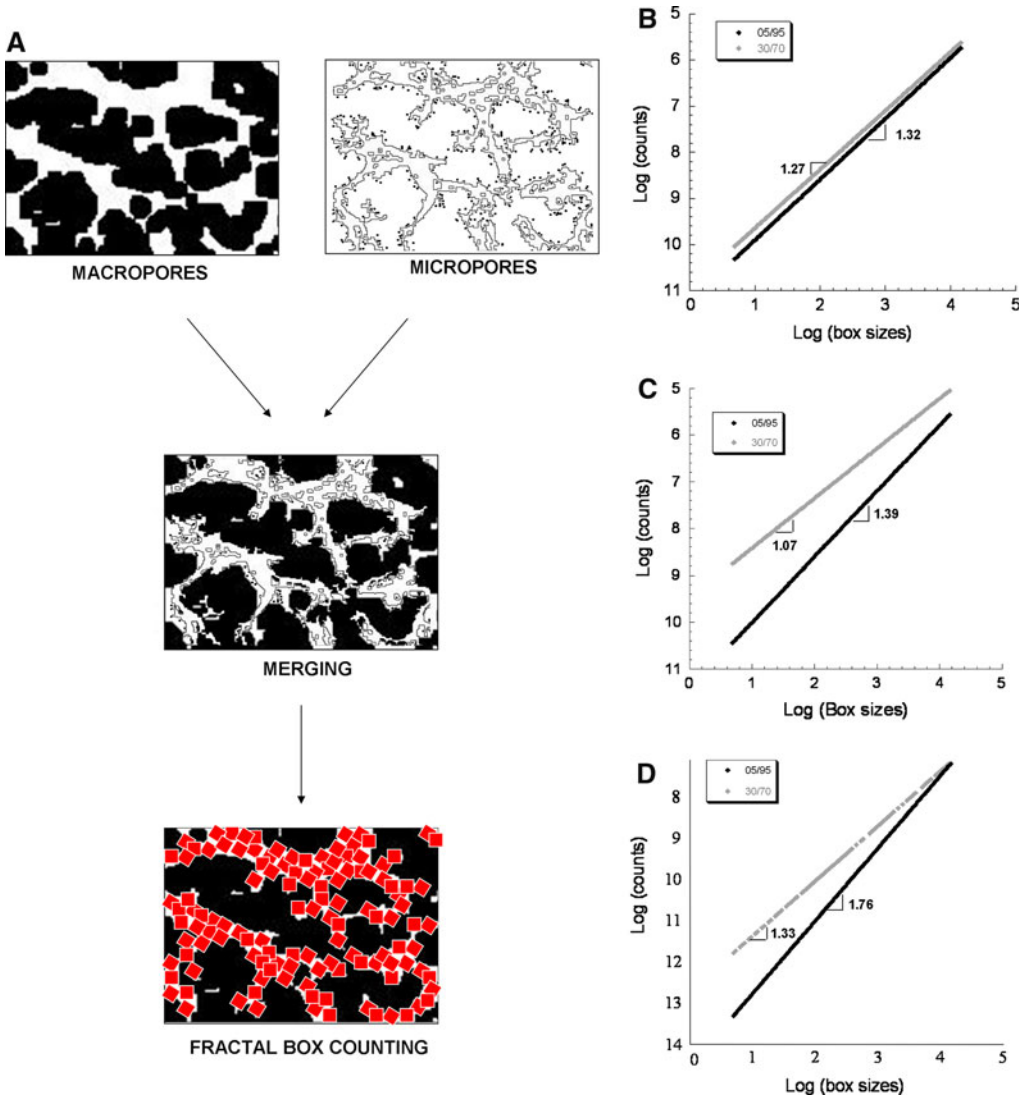

Fig. 6 Evaluation of the pore structure interconnectivity of PCL scaffolds by the calculation of cluster fractal dimension: scheme of box-counting method on representative image (**a**), estimation of percolation cluster size of **b** micro-pore network, **c** macropore network and **d** bi-modal pore network

investigation (i.e., one for a line, two for a plane, etc.), the higher is the interconnection degree of the structure [48, 49]. The procedure adopted herein has been schematically reported (Fig. 6a). IP for fractal dimension calculation was performed on our PCL scaffolds by using ImageJ freeware plug-in, adopting the box counting method, as previously described. The slope of curve depicted in Figs. 6b–d is the fractal dimension of percolating clusters. It is worth to note that it is expected a fractal ranging from 1 to 2, for that the original object is a planar image. Moreover, since two porous populations have been depicted, their fractal dimensions were calculated separately. Curves reported in Fig. 6b represent the application of box counting method to the population of macropores in PCL 5/95 and 30/70 (wt/wt) respectively. As expected, the fractal dimensions of the two percolative clusters is almost the same (slope 1.27–1.32) and the curve are nearly parallel. Indeed, since the macropore percentage is about the same in both scaffolds, and their distribution is absolutely random, there is the same probability that a pore belongs to the percolating cluster.

Instead, the application of box counting method to micropore population (Fig. 6c) shows a decrease in cluster fractal dimension as a function of the curve slope passing from 1.39 to 1.07, in line with micropore fraction variation highlighted by previous quantitative image calculations. Finally, similar elaborations on more complex structures obtained by the merging of isolated micro- and macro-pore images which better represent the structural complexity of the effective three-dimensional scaffold, shows a fractal cluster with dimensions varying from 1.76 to 1.33 as micropore volume fraction decreases (Fig. 6d). All these data concur to indicate that the micro-pores population might control the ID of scaffolds, with the consequent implications in design and preparation of polymeric constructs.

4 Conclusions

In this paper it has been proposed a schematic procedure for the analysis of morphological features of porous scaffolds by the application of image processing and fractal box counting to 2D micrographs extracted from the 3D structures. The major advantages of such technique and the eventual drawbacks due to the eventual limits in image resolution have been explored. Moreover, IP approach was implemented on PCL scaffold by using a self developed Matlab routine, for image segmentation, based on edge detection method. Results have been compared to the manual threshold to validate the algorithm used. Two pore populations with proper characteristics, in terms of pore size and porosity degree, have been individuated, also overcoming the problem of measurement artefacts in soft-matter based scaffolds, of traditionally adopted mercury intrusion techniques. Finally, it has been verified that the estimation of fractal dimension of percolating clusters may result a promising method for evaluating the interconnection degree of complex multi-scaled porous networks. In perspective, these data pave the way for a probabilistic estimation of pore morphological features, which will constitute a powerful tool for the definition of design criteria of scaffolds for tissue engineering.

Acknowledgments This study was financially supported by the IP STEPS EC project, FP6-500465. The authors wish to acknowledge the support obtained from Italian Ministry of University and Research (TISSUENET) for this research. Moreover, they would also like to thank Mr. Maurizio Cotugno for its collaboration during its bachelor master thesis spent in the Institute of Composite and Biomedical Materials and Mr. Paolo Carboni for its support in the image reconstruction.

References

1. Costa MFM. Application of image processing to the characterization of nanostructures. Rev Adv Mater Sci. 2004;6:12–20.
2. Coker DA, Torquato S, Dunsmuir JH. Morphology and physical rpoperties of Fontainebleu sand stone via a tomographic analysis. J Geophys Res. 1996;101:17497–506.
3. Lindquist WB, Lee SM, Coker DA, Jones KW, Spanne P. Medial axis analysis of void structure in three dimensional tomographic images of porous media. J Geophys Res. 1996;101(B4):8297–310.
4. Proussevitch AA, Sahagien DL. Recognition and separation of discrete objects within complex 3D voxalized structures. Comput Geosci. 2001;27(4):441–54.
5. Jones AC, Milthorpe B, Averdunk H, Limaye A, Senden TJ, Sakellariou A, Sheppard AP, Sok RM, Knackstedt MA, Brandwood A, Rohner D, Hutmacher DW. Analysis of D bone ingrowth into polymer scaffolds via micro-computed tomography imaging. Biomaterials. 2004;25(20):4947–54.
6. Moore MJ, Jabbari E, Ritman EL, Lu L, Cumer BL, Widebank AJ, Yoszemki MJ. Quantitative analysis of interconnectivity of porous biodegradable scaffolds with microcomputed tomography. J Biomed Mater Res. 2004;71A:258–67.
7. Cartmel S, Huynh K, Lin A, Nagaraja S, Guldberg R. Quantitative microcomputed tomography of mineralization within three-dimensional scaffolds in vitro. J Biomed Mater Res. 2004;69A(1):97–104.
8. Brumke O, Odenbach S, Beckman F. Quantitative methods for the analysis of syncroton- CT data sets of metallic foams. Eur Phys J Appl Phys. 2005;29(1):73–82.
9. Cooper DML, Turinky AL, Sensen CW, Hellgrimsson B. Quantitative 3D analysis of the canal network in cortical bone by micro-computed tomography. Anat Rec. 2003;274B:169–79.
10. Darling AL, Sun W. 3D microtomographic characterization of precision extruded polycaprolactone scaffolds. J Biomed Mater Res. 2004;70B:311–7.
11. Otsuki B, Takemoto M, Fujibayashi S, Neo M, Kokubo T, Nakamura T. Pore throat size and connectivity determine bone and tissue ingrowth into porous implants: three-dimensional micro-CT based structural analysis of porous bioactive titanium implants. Biomaterials. 2006;27:5892–900.

12. Rüegsegger P, Koller B, Muller R. A microtomographic system for the nanostructure evaluation of bone architecture. Calcif Tissue Int. 1996;58(1):24–9.
13. Hildebrandt T, Rüegsegger P. Quantification of bone microarchitecture with the Structure Model Index. Comput Methods Biomech Biomed Eng. 1997;1:15–23.
14. Van Lenthe GH, Hagenmüller H, Bohner M, Hollister SJ, Meinel L, Müller R. Nondestructive micro-computed tomography for biological imaging and quantification of scaffold–bone interaction in vivo. Biomaterials. 2007;28(15):2479–90.
15. Rajagopalan S, Lu L, Yaszemski MJ, Robb RA. Optimal segmentation of microcomputed tomographic images of porous tissue-engineering scaffolds. J Biomed Mater Res A. 2005;75: 877–87.
16. Oh SH, Park IK, Kim JM, Lee JH. In vitro and in vivo characteristics of PCL scaffolds with pore size gradient fabrication by a centrifugation method. Biomaterials. 2007;28:1404–13.
17. Moquet V, Bòacher S, Pirard R, Pirard JP, Jerome R. Characterization of porous polylactide foams by image analysis and impedance spectroscopy. Langmuir. 2000;16:10463–70.
18. Grant PV, Voz CM, Tomlins PE, Mikvalovska L, Jones S, Mikalovsky S, Vadgama P. Surface chemistry in biomedical and environmental science part 2. The Netherlands: Springer; 2006. pp. 215–28.
19. Winslow DN. Advances in experimental techniques for mercury intrusion porosimetry. In: Matjevic E, Good RJ, editors. Surface and colloid science. New York: Plenum Press; 1984. p. 259–82.
20. Zein I, Hutmacher DW, Tan KC, Teoh SH. Fused deposition modeling of novel scaffold architectures for tissue engineering applications. Biomaterials. 2002;23(4):169–85.
21. Li CT. Multiresolution image segmentation integrating Gibbs sampler and region merging algorithm. Signal Process. 2003; 83(1):67–78.
22. Mather ML, Morgan SP, White LJ, Tai H, Kockenberg W, Crowe JA. Image-based characterization of foamed polymeric tissue scaffolds. Biomed Mater. 2008;3:1–11.
23. Malpica N, Solorzano C, Vaquero J, Santos A, Vallcorba I, Garcia-Sagredo J, F Pozo. A multichannel watershed-based algorithm for supervise texture segmentation. Cytometry. 1997; 28:289–97.
24. Sijbers J, Verhoye M, Scheunders A, Van der Linden A, Van Dyck D, Raman E. Watershed-based segmentation of 3D MR data for volume quantification. Magn Reson Imaging. 1997;15(6):679–88.
25. Cates JE, Whitaker RT, Jones GM. Case study: an evaluation of user-assisted hierarchical watershed segmentation. Med Image Anal. 2005;9(6):566–78.
26. Sezgin M, Sankur B. Survey over image thresholding techniques and quantitative performance evaluation. J Electron Imaging. 2004;13(1):146–65.
27. Whang K, Thomas CK, Nuber G, Heoly KE. A novel method to fabricate bioresorbable scaffolds. Polymers. 1995;36:837.
28. Heoly KE, Tsai D, Kim JE. Osteogenic cell attachment to degradable polymers. Mater Res Soc Symp Proc. 1992;252: 109–14.
29. Murphy WL, Dennis RG, Kileny JL, Mooney DJ. Salt fusion: an approach to improve pore interconnectivity within tissue engineering scaffolds. Tissue Eng. 2002;8(1):43–52.
30. Mathieu LM, Mueller TL, Bourban PE, Pioletti DP, Müller R, Månson JAE. Architecture and properties of anisotropic polymer composite scaffolds for bone tissue engineering. Biomaterials. 2006;27(6):905–16.
31. Guarino V, Taddei P, Di Foggia M, Fagnano C, Ciapetti G, Ambrosio L. Influence of hydroxyapatite particles on in vitro degradation behaviour of poly ε-caprolactone-based composite scaffolds. Tissue Eng. 2009;15(11):3655–68.
32. Smith TG Jr, Lange GD, Marks WB. Fractal methods and results in cellular morphology. J Neurosci Methods. 1996;69:1123–26.
33. Schugens C, Maquet V, Grandfils C, Jerome R, Teyssie P. Biodegradable macroporous polylactide implants for cell transplantation: I. Preparation of polylactide foams by solid-liquid phase separation. Polymer. 1996;37:1027–38.
34. Salerno A, Guarnieri D, Iannone M, Zeppetelli S, Di Maio E, Iannace S, Netti PA. Engineered l-bimodal poly(e-caprolactone) porous scaffold for enhanced hMSC colonization and proliferation. Acta Biomater. 2009;5(4):1082–93.
35. Guarino V, Causa F, Ambrosio L. Porosity and mechanical properties relationship in PCL based scaffolds. J Appl Biomater Biomech. 2007;5(3):149–57.
36. Ho ST, Hutmacher DW. A comparison of micro-CT with other techniques used in the characterization of scaffolds. Biomaterials. 2006;27:1362–76.
37. Guarino V, Causa F, Netti PA, Ciapetti G, Pagani S, Martini D, Baldini N, Ambrosio L. The role of hydroxyapatite as solid signals on performance of PCL porous scaffolds for bone tissue re generation. J Biomed Mat Res Appl Biomater. 2008;86B:548–57.
38. Srinivasan R, Lu L, Yaszemski MJ, Robb RA. Optimal segmentation of microcomputed tomographic images of porous tissue-engineering scaffolds. J Biomed Mater Res A. 2005; 75(4):877–87.
39. Reed AH, Briggs KB, Lavoie DL. Porometric properties of a siliciclastic marine sand: a comparison of traditional laboratory measurements with image analysis and effective medium theory modelling. IEEE J Ocean Eng. 2002;27:581–92.
40. Ehrlich R, Kennedy SK, Crabtree SJ, Cannon RL. Petrographic image analysis I. Analysis of reservoir pore complexes. J Sediment Pet. 1984;54:1365–78.
41. White JV, Kirkland BL, Gournay JP. Quantitative porosity determination of thin sections using digitized images. J Sediment Res. 1998;68:220–2.
42. Reed AH, Pandey RB, Lavoie DL. Fractal dimensionality of pore and grain volume of a siliciclastic marine sand. Int J Mod Phys C. 2000;11:1555–9.
43. Yamaguchi T, Hashimoto S. Image processing based on percolation model. IEICE Trans Inf Syst. 2006;E89-D(7):2044–52.
44. Hussain I, Reed TR. A bond percolation-based model for image segmentation. IEEE Trans Image Process. 1996;6(12):1698–704.
45. Craciunescu OI, Das SK, Clegg ST. Dynamic contrast-enhanced MRI and fractal characteristics of percolation clusters in two-dimensional tumor blood perfusion. Trans ASME J Biomech Eng. 1999;121:480–6.
46. Stauffer D, Aharony A. Introduction to percolation theory. Philadelphia: Taylor and Francis; 1994.
47. Mandelbrot BB. The fractal geometry of nature. San Francisco: CA Freeman; 1982. pp. 468–69.
48. Orford JD, Walley WB. The use of fractal dimension to quantify the morphology of irregular shaped particles. Sedimentology. 1983;30:655–68.
49. Oh W, Lindquist WB. Image thresholding by indicator kriging. IEEE Trans Pattern Anal Mach Intell. 1999;21(7):590–602.